

SMR: 1513/9

**10TH CONFERENCE ON HOPPING
AND RELATED PHENOMENA**

(1 - 4 September 2003)

***"Study on the Mechanism of Proton
Conductivity in Zero-Dimensional
Hydrogen-Bonded Crystals $M_3H(XO_4)_2$ with
 $M=K, Rb, Cs$ and $X=S, Se$ "***

presented by:

H. Kamimura
Tokyo University of Science
Japan

These are preliminary lecture notes, intended only for distribution to participants.

Study on the Mechanism of Superionic Conduction in the Zero-Dimensional Hydrogen-Bonded Crystals $M_3H(XO_4)_2$ with $M=Rb, Cs$ and $X=S, Se$

Hiroshi Kamimura
Tokyo University of Science

Introduction

- Recently the superionic hydrogen-bonded crystals of ferroelastic $M_3H(XO_4)_2$ type have been extensively studied.
- In this talk I would like to discuss the mechanism of superionic conduction in the paraelastic phase ($T > T_c$) and also near and below the phase transition.

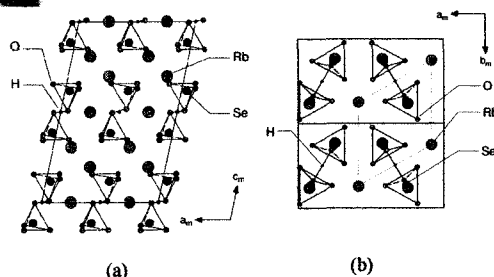
Outline of the talk

- My talk consists of two parts:
 - In the first part I will propose a new mechanism of superionic conduction in the paraelastic phase ($T > T_c$) due to coherent tunneling of protons, based on recent experimental results.
 - In the second part I will discuss a mechanism of proton conduction near and below the phase transition, by taking account of fluctuation effects.

Collaborators

- Experiments**
 - Yasumitsu Matsuo (TUS)
 - Seiichiro Ikehata (TUS)
 - Masaru Komukae (TUS)
 - Toshio Osaka (TUS)
- Theory**
 - Takuo Ito (Fujitsu)
 - Masaru Watanabe (Noshiro Tech. High School)

Crystal Structure of $Rb_3H(SeO_4)_2$



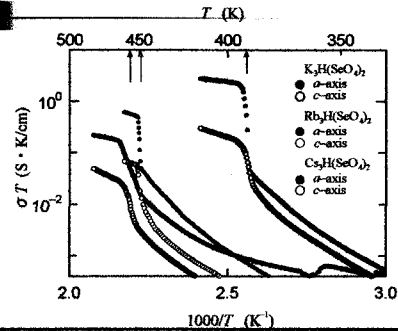
Explanation of the Crystal Structure

- The figure (a) shows a projection of the crystal structure of the ferroelastic phase ($T < T_c$) on the a - c plane.
- We note that the top and bottom oxygen of the neighboring tetrahedrons lie at the same height along the c -axis and that a hydrogen bond is formed in between these top and bottom oxygen.
- These hydrogen bonds are isolated shown here for the ferroelastic phase. Such isolation can be seen clearly in the figure (b), showing a projection of the crystal structure on the a - b plane.

Explanation of the Crystal Structure (continue)

- In the paraelastic phase ($T > T_c$), each tetrahedron is tilted so as for Rb, Se and O to stand in line perpendicular to the a - b plane (i.e. c^* -axis).
- As a result a crystal structure in the paraelastic phase has the three-fold axes along the c^* -axis and the length of the hydrogen bonds becomes equal. We call this phase a *super-ionic phase*.
- A unit cell of tetragonal shape in the monoclinic system ($T < T_c$) changes to a rhombohedral shape surrounded by the red line.
- The space group of the *super-ionic phase* is R3m.

Temperature dependence of electrical conductivity in the $M_3H(\text{SeO}_4)_2$ type crystals ($M=K, Rb, Cs$)



Features of Observed Conductivity in the super-ionic phase ($T > T_c$)

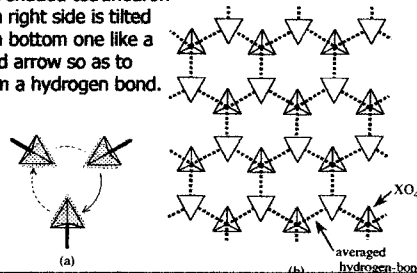
The slide shows the temperature dependence of electrical conductivity observed for $Rb_3H(\text{SeO}_4)_2$.

In the *super-ionic phase* ($T > T_c$),

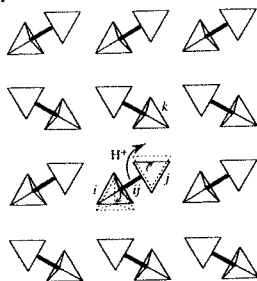
- $\log(\sigma T)$ is proportional to $1/T$, that is the Arrhenius-type conduction.
- The conductivity is as high as 10^{-2} to 10^{-4} S/cm.
- Conductivity along the a -axis is 10^2 times larger than that along the c -axis.
- Thus $M_3H(\text{XO}_4)_2$ crystals display a quasi-two dimensional conduction in the *super-ionic phase*.
- The activation energy is about 0.2 eV along the a -axis and about 0.4 eV along the c -axis.

First Part: Origin of Proton Conduction in the super-ionic phase ($T > T_c$)

In figure (a) top oxygen in a shaded tetrahedron at a right side is tilted to a bottom one like a solid arrow so as to form a hydrogen bond.

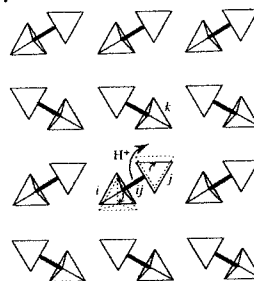


Mechanism of Proton conduction in the super-ionic phase ($T > T_c$): Formation of two ionic states



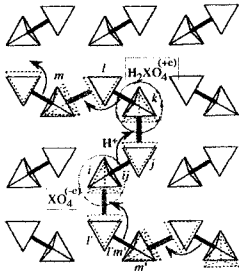
Suppose a hydrogen-bond ij between two tetrahedrons marked by i and j is broken thermally, by the tilt of tetrahedron j toward k . Then proton H^+ at ij hops to an interstitial position between j and k to form a new hydrogen bond.

Mechanism of Proton conductivity in the super-ionic phase (continue): Formation of two ionic states



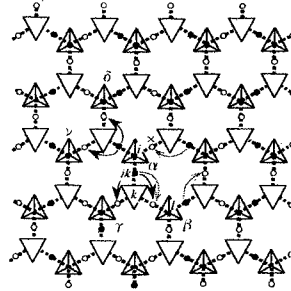
Simultaneously an electron separated from a proton is accommodated at tetrahedron i .

Formation of two kinds of ionic states, $H_2XO_4^{(+e)}$ and $XO_4^{(-e)}$



Thus two kinds of ionic states, $H_2XO_4^{(+e)}$ (red circle) and $XO_4^{(-e)}$ (green circle) are created thermally. These ionic states contribute to superionic conduction.

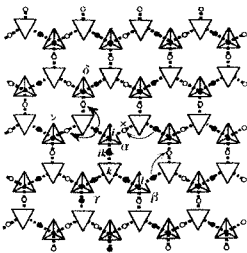
Theoretical Model: Characterization of $H_2XO_4^{(+e)}$ state



$H_2XO_4^{(+e)}$ ionic state is characterized by its position and orientation as α, β, γ and δ .

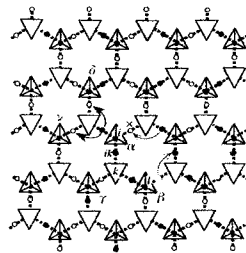
- vacant site of proton
- occupied site of proton

Theoretical Model: Motion of $H_2XO_4^{(+e)}$ ionic state

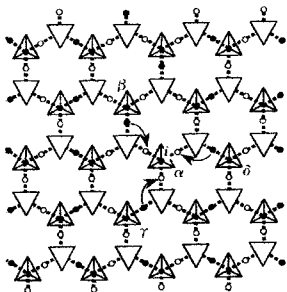


When either of two protons in the state α is transferred, state α changes to $\beta,$ or γ . Proton transfer to a site indicated by x is not allowed.

Demonstration of itinerancy of $H_2XO_4^{(+e)}$ ionic state



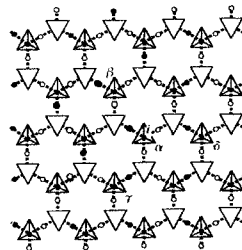
Theoretical Model: Characterization of $XO_4^{(-e)}$ ionic state



$XO_4^{(-e)}$ ionic state is characterized by its position and orientation as $\alpha, \beta,$ and γ .

- vacant site of proton
- occupied site of proton

Demonstration of itinerancy of $XO_4^{(-e)}$ ionic state

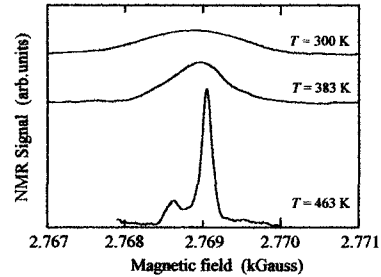


Summary for the itinerant motions of two ionic states

- The motion of two ionic states occurs by the interplay between the proton tunneling and tilting of top and bottom oxygen. As a result the two kind of ionic states moves resonantly, changing their states, say from α to β , and then to γ , etc.
- Consequently a band-like state is formed for each of $H_2XO_4^{(±)}$ and $XO_4^{(±)}$ ionic states.

Experimental evidence for coherent motion of proton:

1H -NMR absorption line in $Rb_3H(SeO_4)_2$



Explanation of NMR Data

- This figure shows the 1H -NMR absorption line in the $Rb_3H(SeO_4)_2$ crystal for various temperatures.
- It is evident that the NMR absorption line in the *super-ionic phase* becomes sharper than that at room temperature. The NMR line width in the *super-ionic phase* becomes about 0.3 G, while the line width at room temperature is 1.1G.
- We can say that the sharpening of the NMR line for $T > T_c$ is the motional narrowing effect due to the itinerant motion of proton in the *super-ionic phase*.

Model Hamiltonian

In order to describe the coherent motion of $H_2XO_4^{(±)}$ states, we propose the model Hamiltonian:

$$H = \sum_l \sum_k \sum_i \Gamma a_{kl}^\dagger a_{ik} \left(\sum_j a_{ij}^\dagger a_{ij} - 1 \right),$$

Γ : Transfer interaction of a proton between adjacent sites

a_{ij}^\dagger : Creation operator of a proton at the site ij

The factor in (.....) means that only either of two protons in $H_2XO_4^{(±)}$ at i site can transfer.

Expression for ionic current

The ionic current due to a coherent motion of a Proton is given by the following equation:

Current

$$J = \left(\frac{iq}{\hbar} \right) \sum_{i,j} \Gamma R_{ij} a_{jk}^\dagger a_{ij} \left(\sum_l a_{il}^\dagger a_{il} - 1 \right)$$

where $R_{ij} = R_j - R_i$.

When a proton hops from ij site to jk site by transfer interaction Γ , a charge q of $H_2XO_4^{(±)}$ or $XO_4^{(±)}$ moves from site i to site j , R_{ij} .

Method for Calculation of the Density of states $\rho(E)$

We calculate the density of states for two kinds of itinerant ionic states $H_2XO_4^{(±)}$ and $XO_4^{(±)}$ based on the model Hamiltonian. For this purpose we introduce the Green's function defined by

$$\begin{cases} G_{\beta\alpha}^{(+)}(E) = \langle \beta | \frac{1}{E + i\epsilon - H} | \alpha \rangle, & \epsilon = +0 \\ G_{\beta\alpha}(E) = -\frac{1}{\pi} \text{Im} G_{\beta\alpha}^{(+)}(E) \implies \rho(E) \end{cases}$$

(next page \Rightarrow)

Density of states $\rho(E)$ for the itinerant ionic states

$$\rho(E) = \frac{3}{2\pi} \text{Im} G_{\alpha\alpha}(E)$$

Matrix elements of the Hamiltonian

The present model Hamiltonian has an interesting feature. That is, the Hamiltonian has the matrix elements only for the states related to the neighboring sites, as seen below.

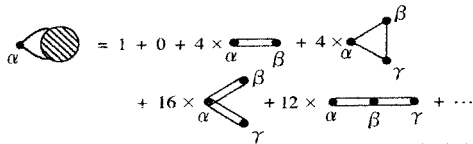
$$\langle \beta | H | \alpha \rangle = \begin{cases} T: & \text{for } |\alpha\rangle \text{ \& } |\beta\rangle \text{ being neighboring sites} \\ 0 & \text{otherwise} \end{cases}$$

Expansion of Green's Function

Expand in terms of H/z ($z = E + i\epsilon$)

$$zG_{\alpha\alpha}^{(+)}(E) = 1 + \frac{H_{\alpha\alpha}}{z} + \sum_{\beta} \frac{H_{\alpha\beta}H_{\beta\alpha}}{z^2} + \sum_{\gamma} \sum_{\beta} \frac{H_{\alpha\gamma}H_{\gamma\beta}H_{\beta\alpha}}{z^3} + \dots$$

Diagrammatic representation of the above $zG_{\alpha\alpha}(E)$

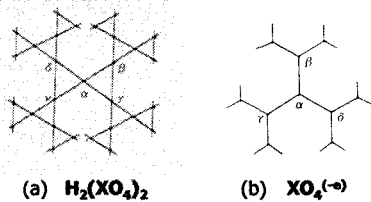


Interaction Map

As seen in the previous slide,

- $(zG_{\alpha\alpha}^{(+)}(E) - 1)$ is equal to the sum of all closed paths which start from a state α and end at the starting state α via intermediate states β, γ, δ , etc., since only the matrix elements of H between nearest neighbor states.
- Thus we have to find such closed paths.
- This is called an *interaction map*.

Interaction maps for $H_2XO_4^{(+e)}$ and $XO_4^{(-e)}$



Interaction maps basically belong to the Bethe lattice (Cayley tree).

Recursion Method by Haydock et al

- As the method of summing up the closed paths described by the Bethe lattice, the recursion method developed by Haydock, Heine and Kelly is suitable.
- R. Haydock, V. Heine and M.J. Kelly, J. Phys. C 5 (1972) 2845; *id.* C 8 (1975) 2591.
- Thus we have employed it.
- According to this method, the diagonal element of Green's function for the Bethe lattice is expressed in the form of continued fraction, as shown in the next slide.

Green's function in the form of the continued fractional representation

$$G_{00}^{(+)}(z) = \frac{1}{z - a_0 - \frac{b_1^2}{z - a_1 - \frac{b_2^2}{z - a_2 - \dots - \frac{b_{n_0}^2}{z - a_{n_0} - b_{n_0}^2 t(z)}}}}$$

with $t(z) = \frac{1}{z - a_{\infty} - b_{\infty}^2 t(z)}$

In an ordinary case, a_n and b_n approach quickly to constant values a_{∞} and b_{∞} when a step n exceeds a certain value n_0 . Thus we can terminate the continued fraction by putting $a_{n_0} = a_{\infty}$ and $b_{n_0} = b_{\infty}$.

Thus
$$t(z) = \frac{(z - a_{\infty}) - \sqrt{(z - a_{\infty})^2 - 4b_{\infty}^2}}{2b_{\infty}^2}$$

Exact solutions of $t(z)$ for Bethe lattice

For NO_3^- ionic state
 $a_n = 0$ for all n 's
 $b_1 = \sqrt{3} \Gamma$
 $b_2 = \sqrt{2} \Gamma$
 $b_n = \sqrt{2} \Gamma$ for $n \geq 2$

Thus
$$t(z) = z - (\sqrt{2}\Gamma)^2 t(z)$$

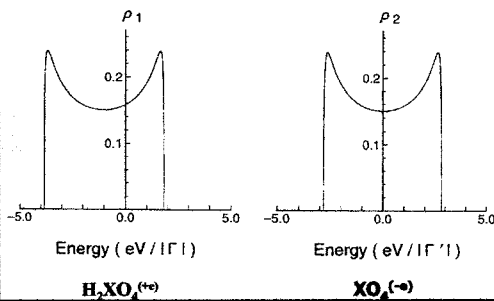
From this we obtain
$$t(z) = z - \frac{\sqrt{z^2 - 8\Gamma^2}}{11^2}$$

Hence
$$G_{00}^{(+)}(z) = \frac{1}{z - \frac{1}{z - 2\Gamma^2}}$$

with $z = E + i\epsilon$

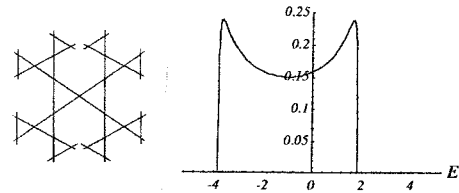
$$\rho(E) = -\frac{3}{2\pi} \text{Im} G_{00}^{(+)}(E)$$

Calculated Density of states for $\text{H}_2\text{XO}_4^{(+e)}$ and $\text{XO}_4^{(-e)}$



Remarks on Density of states for $\text{H}_2\text{XO}_4^{(+e)}$

Why is the center of DOS for $\text{H}_2\text{XO}_4^{(+e)}$ shifted?



Answer: The existence of loops in interaction map.

Kubo formula for ionic mobility

$$\mu = \left(\frac{\pi \hbar}{2qkT} \right) \int e^{-E/kT} \Xi(E) dE / \int e^{-E/kT} \rho(E) dE$$

$$\Xi(E) = -\frac{1}{N} \sum_{\alpha} \sum_{\beta} \sum_{\gamma} \sum_{\delta} G_{\alpha\delta}(E) H_{\delta\gamma} \vec{R}_{\delta\gamma} G_{\gamma\beta}(E) H_{\beta\alpha} \vec{R}_{\beta\alpha}$$

In order to calculate the mobility, we have first to calculate the off-diagonal elements of the Green's function $G_{\alpha\beta}$. For this purpose we expand it in terms of H/z .

Expansion of off-diagonal Green's function in terms of H/z

The result is shown below:

$$zG_{\beta\alpha}^{(+)}(E) = \delta_{\beta\alpha} + \frac{1}{z} H_{\beta\alpha} + \sum_{\nu=1}^{\infty} \frac{1}{z^{\nu+1}} \sum_{\gamma_1} \sum_{\gamma_2} \dots \sum_{\gamma_{\nu}} H_{\beta\gamma_{\nu}} \dots H_{\gamma_2\gamma_1} H_{\gamma_1\alpha}$$

where $z = E + i\epsilon$.

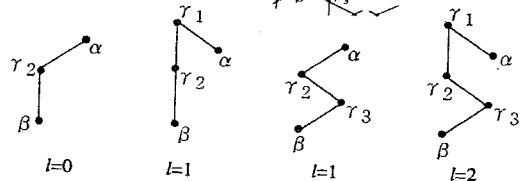
Remarks on the calculation of mobility

- In calculating the Green's function, we sum up all the paths which start from a state α and end at a state β via intermediate states.
- Among the paths, the paths which have no any common intermediate states are called "irreducible routes". When the length of the shortest paths between α and β is m steps, $G_{\alpha\beta}$ is denoted as $G_m(E)$.

Four irreducible routes for $m = 2$

Here l represents the difference between the steps of each irreducible route and that of the shortest one ($l = 0$).

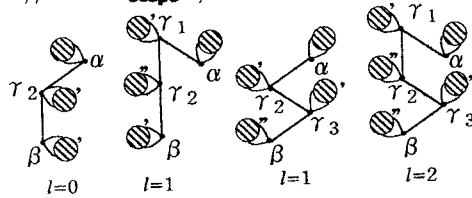
Case of $H_2(XO_4)_2^{(+)}$. Interaction map is shown



Diagrams of $zG_{m=2}^{(+)}$

(ξ' does not contain a state adjacent to γ_2 , while ξ'' does not contain γ_2 and γ_1 on the way.)

α, β $m=2$ steps ;



where $\xi = \alpha \rightarrow \alpha$ ($=zG_{\alpha\alpha}^{(+)}$) $\xi' = \alpha \rightarrow \gamma_1 \rightarrow \alpha$ $\xi'' = \alpha \rightarrow \gamma_1 \rightarrow \gamma_2 \rightarrow \alpha$

General Expression of $zG_{\alpha\beta}^{(+)}(E)$

$$zG_{\alpha\beta}^{(+)}(E) = zG_m^{(+)} = \sum_{\ell=0}^m m C_{\ell} \xi \left(\frac{\Gamma}{z}\right)^{m+\ell} \xi^m \xi^{\ell}$$

$$\xi = \alpha \rightarrow \alpha \quad \xi' = \alpha \rightarrow \gamma_1 \rightarrow \alpha \quad \xi'' = \alpha \rightarrow \gamma_1 \rightarrow \gamma_2 \rightarrow \alpha$$

Calculated Results for mobility

Mobility (Assuming both $|\Gamma|$ and $|\Gamma'| \ll kT$)

$$\begin{cases} \mu = \frac{q|\Gamma|R^2}{\hbar kT} \times 1.070 & : H_2XO_4^{(+e)} \\ \mu' = \frac{|q'|\Gamma'R^2}{\hbar kT} \times 1.066 & : XO_4^{(-e)} \end{cases}$$

Here q and q' are the effective charges of $H_2XO_4^{(+e)}$ and $XO_4^{(-e)}$ respectively.

Einstein Relation for mobility

Our results for mobility has the form of the Einstein relation in its temperature dependence. From this we can derive the diffusion constant for $H_2XO_4^{(+e)}$ as follows;

$$D = \frac{|\Gamma|R^2}{\hbar} \times 1.07 \quad \tau = \frac{\hbar}{|\Gamma|}$$

where τ is a scattering time. Since two kinds of ionic states are formed thermally, the density of ionic states are given by the Boltzmann distribution;

$$n = n_0 e^{-E_a/kT} \quad \therefore \sigma \propto \frac{e^{-E_a/kT}}{T}$$

Estimated values of mobility and conductivity

For $\text{Rb}_3\text{H}(\text{SeO}_4)_2$, $E_a = 0.26\text{eV}$, $R = 5.8 \times 10^{-8}\text{cm}$, and $T_c = 450\text{K}$. Assuming that $q = |q'| = e$, $n_0 = 10^{22}\text{cm}^{-3}$, and $|\Gamma| = |\Gamma'| = 10^{-5}\text{eV}$, we estimate the mobility;

$$\mu_{\text{total}} = \mu + \mu' = 2.6 \times 10^{-4} [\text{cm}^2/\text{Vsec}]$$

$$n \sim 10^{+19} [\text{cm}^{-3}]$$

$$\sigma = nq(\mu + \mu') \sim 10^{-3} [\Omega^{-1}\text{cm}^{-1}]$$

The above estimated values are in good agreement with observed values.

Arrhenius' equation

We have showed that

Conductivity follows Arrhenius' equation .

$$\sigma = qn(\mu + \mu') \rightarrow (\sigma = A e^{-E_a/kT}/T)$$

The origin for it is due to the T-dependence of the concentration of two kinds of excited ionic states.

Summary of the First Part:

A new mechanism of proton conduction in the superionic phase

- The key features of the mechanism are the following two:
- (1) Two kinds of ionic states $\text{H}_2\text{XO}_4^{(+)}$ and $\text{XO}_4^{(-)}$ are formed thermally by breaking a hydrogen bond. This thermal activation process is the origin of the observed Arrhenius' equation in the temperature dependence of conductivity.

Summary(Continue)

- (2) The $\text{H}_2\text{XO}_4^{(+)}$ and $\text{XO}_4^{(-)}$ states move coherently as a result of successive proton tunneling among hydrogen bonds. In this sense the proton conduction in the superionic phase has a quantum mechanical nature.
- In this context we calculated conductivity by the Kubo formula. Nevertheless, the obtained mobility has the form of Einstein relation.
- Agreement between theory and experiment is fairly good.

New Mechanism of Ionic Conductivity in Hydrogen-Bonded Crystals $M_3H(XO_4)_2$ [$M=Rb, Cs, X=S, Se$]

Takuo ITO* and Hiroshi KAMIMURA

*Institute of Physics, Graduate School of Science, Science University of Tokyo,
1-3, Kagurazaka, Shinjuku-ku, Tokyo 162-8601*

(Received June 11, 1997)

A model for the mechanism of ionic conductivity in the high temperature paraelastic phase of $M_3H(XO_4)_2$ [$M=Rb, Cs, X=S, Se$] type crystals is proposed. The key features of the conduction mechanism are the following; (1) two kinds of defect states, $H_2XO_4^{(+e)}$ and $XO_4^{(-e)}$, are formed thermally by breaking of a hydrogen-bond, (2) the $H_2XO_4^{(+e)}$ defect state and the $XO_4^{(-e)}$ defect state move coherently from an XO_4 tetrahedron to a distant XO_4 as the result of successive proton tunneling among hydrogen-bonds. The density of states and the mobility are calculated for the coherent motions of these defect states by the recursion method and the Kubo formula, respectively. The density of states shows the characteristic feature of the Bethe lattice, i.e., the twin peak structure due to self-similarity, while the conductivity is obtained as an order of a magnitude of $10^{-3}\Omega^{-1}cm^{-1}$ at the ferroelastic transition temperature, consistent with experiments.

KEYWORDS: ionic conductivity, paraelastic phase, hydrogen-bond, proton tunneling, Bethe lattice

§1. Introduction

Hydrogen-bonded materials, whose nature is closely related to the behavior of protons in hydrogen-bonds, exhibit a number of interesting phenomena. For example, a large isotope effect by substituting deuteron for hydrogen is well known in hydrogen-bonded ferroelectric or antiferroelectric materials, and have been investigating from a number of theoretical aspects¹⁻⁵⁾ and experimental ones.^{6,7)} On the other hand, it has been reported that $M_3H(XO_4)_2$ [$M=Rb, Cs, X=S, Se$] and $MHXO_4$ type dielectric crystals exhibit a ferroelastic phase transition at high temperatures, and the anomalous large increase of electrical conductivity near the phase transition temperature has been observed.⁸⁻¹³⁾ X-ray diffraction studies by Baranov *et al.* indicate that the ferroelastic phase transition is due to the disordering in the geometrical arrangement of hydrogen-bonds. NMR studies¹⁴⁻¹⁶⁾ show that the charge carriers are the protons. Thus the transport phenomenon in $M_3H(XO_4)_2$ and $MHXO_4$ is associated with the dynamical behavior of protons among the hydrogen-bonds. This has aroused keen interests as a new type of superionic conductors. Plakida and Salejda¹⁷⁾ proposed a phenomenological theory of the ferroelastic phase transition and transport phenomena in $Rb_3H(SeO_4)_2$.

Figure 1(a) shows a schematic view of the crystal structure of the $M_3H(XO_4)_2$ projected on the ab plane at room temperature, where M atoms are not shown for simplicity. This material is composed of XO_4 tetrahedra. These tetrahedra form XO_4-H-XO_4 dimers by hydrogen-bonds in the ferroelastic phase, and these structurally

isolated XO_4-H-XO_4 dimers form an ordered structure. The space group belongs to $A2/a$. In this material the hydrogen-bonds do not form a network, but a domain structure so that one needs not take account of "ice rule". When the temperature is increased, an order-disorder phase transition as to the system of hydrogen-bonds occurs, and the space group changes to $R\bar{3}m$. This is called a ferroelastic phase transition. In the vicinity of the phase transition temperature T_c , the electrical conductivity rapidly increases, and it is described by a power law as for the temperature dependence. In a paraelastic phase above T_c the conductivity is exceedingly high as ionic conductors. In $Rb_3H(SeO_4)_2$, for example, while low-temperature conductivity is of approximately $10^{-8}\Omega^{-1}cm^{-1}$ at $T = 300$ K, the conductivity reaches up to the value of $5 \times 10^{-3}\Omega^{-1}cm^{-1}$ along the a or b axis at $T_c = 450$ K. The high-temperature conductivity is fitted well by the Arrhenius' equation, and exhibits two-dimensional character, in which the conductivity along the a or b axis is $20 \sim 50$ times higher than that along the c axis.¹⁸⁾ Such transport phenomenon has been understood so far in the following way:⁹⁾ Here we pay attention to the conduction within a layer shown in Fig. 1(a), reflecting an anisotropic behavior of the conductivity. When the temperature is increased from room temperature, the XO_4 tetrahedra start to rotate in the vicinity of T_c , so as for an oxygen atom responsible for the formation of a hydrogen-bond of each tetrahedron to tilt toward a respective direction of the three neighboring XO_4 tetrahedra. Here we call the oxygen atom participating in a hydrogen-bond the top oxygen for each XO_4 . This orientational disordering of the tetrahedra causes the breaking of hydrogen-bonds and the formation of new ones when the top oxygen of a tetrahedron is tilted and the tetrahedron is simultaneously displaced

* Present address: ANALYSIS LABORATORY, TOSHIBA MICROELECTRONICS Corp., 1, Komukai Toshiba-cho, Saiwai-ku, Kawasaki-shi 210-0901.

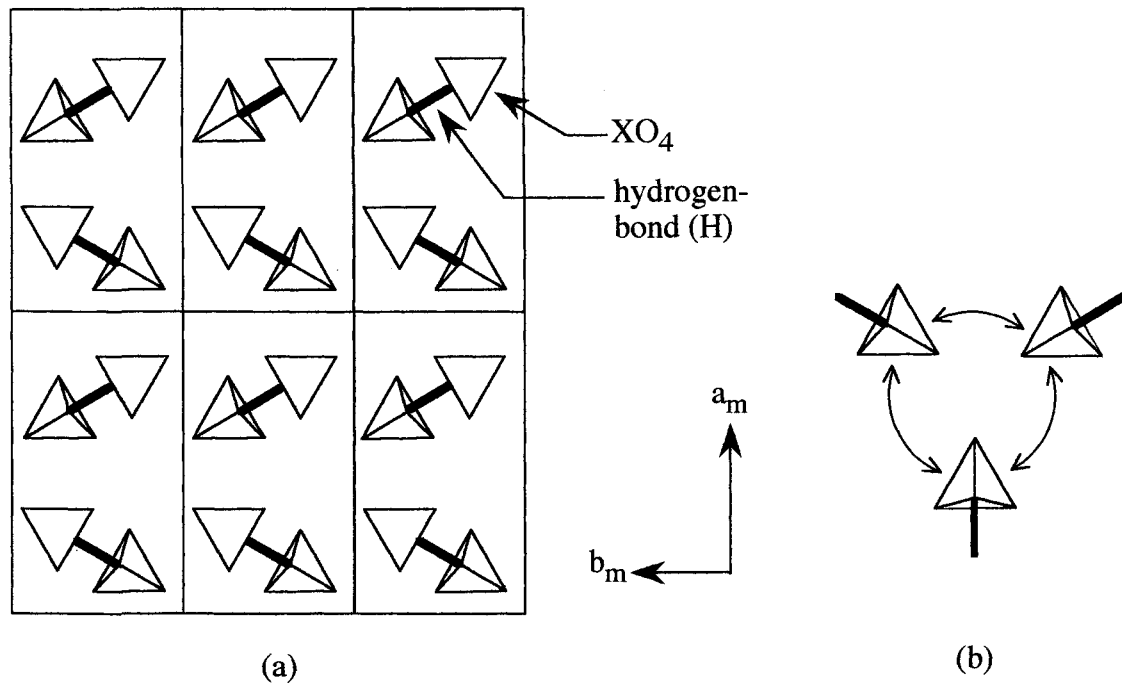


Fig. 1. (a) Projection of the crystal structure of the $M_3H(XO_4)_2$ [$M=Rb, Cs, X=S, Se$] in the room temperature phase on the ab plane. M atoms are not shown for simplicity. (b) Schematic representation of the orientational disordering of each tetrahedron in a crystal, and successive breaking and formation of hydrogen-bonds in the high temperature phase.

toward a neighboring one in order to form a hydrogen-bond newly as shown in Fig. 1(b). This gives rise to the disorder as to the available sites for protons among the hydrogen-bonds. Since the distance between the neighboring XO_4 tetrahedra is nearly equal, the protons can hop among the three structurally equivalent positions in the hydrogen-bonds, resulting in the high electrical conductivity as stated above.

However, even in the disorder phase of protonic positions, there exists a unique correlation between the rotational displacement of XO_4 tetrahedra and the transfer of protons among the hydrogen-bonds. Thus the above transport phenomenon is different from a simple diffusion of protons in ordinary ionic conductors.

In this context we propose a new mechanism of proton conduction in the paraelastic phase by taking into account the interplay between the transfer of protons and the displacement of XO_4 tetrahedra. Then we develop a formula to calculate the density of states and conductivity based on the new mechanism.

§2. A Mechanism of Ionic Conductivity

In this section we describe a mechanism of ionic conductivity of the $M_3H(XO_4)_2$. In the high temperature paraelastic phase, the tetrahedra rotate as stated above, and the geometrical arrangement of the hydrogen-bonds is random. In order to describe the correlated behavior of the protons and of the rotation of the tetrahedra, let us start with a certain arrangement of hydrogen-bonds shown in Fig. 2(a), where XO_4 -H- XO_4 dimers are represented by the thick solid lines. Suppose a hydrogen-bond between two tetrahedra marked by i and j is broken thermally, by the rotational displacement of each top oxygen as shown by the short arrows in Fig. 2(a). Then, when j

is tilted and displaced toward a neighboring tetrahedron, say k , as shown by the dotted lines in this figure, the proton in the hydrogen-bond denoted by ij hops to an interstitial position between the tetrahedra j and k as shown by the arrow, and then tetrahedron k is tilted to j so as for the energies before and after a hop to be equal with each other. Simultaneously the electron separated from the proton is accommodated in the tetrahedron i . As a result two kinds of defect states, $H_2XO_4^{(+e)}$ and $XO_4^{(-e)}$, are formed in the paraelastic phase, as indicated in the dotted circles as shown in Fig. 2(b). The formation process of defect states is of the thermal activation type, because the breaking of the hydrogen-bond is caused by the thermal rotational motion of the tetrahedra. In the $H_2XO_4^{(+e)}$ defect state, two hydrogen-bonds denoted by the thick solid and gray lines are attached to the top oxygen, while in the $XO_4^{(-e)}$ defect state there are no hydrogen-bonds. The $(+e)$ and $(-e)$ represent the extra charges yielded in the respective one of the two tetrahedra when the hydrogen-bond is broken.

First we shall pay attention to the $H_2XO_4^{(+e)}$ defect state. When a new hydrogen-bond is formed between j and k , this brings about the breaking of the hydrogen-bond between the tetrahedra k and l . Then, when l is tilted to a neighboring tetrahedron, say m , an extra proton in the hydrogen-bond kl tunnels to an interstitial position between the tetrahedra l and m , because the energies before and after the tunneling of a proton is equal. As a result the $H_2XO_4^{(+e)}$ defect state which was originally located at k moves to the tetrahedron m . In the same way, the $XO_4^{(-e)}$ defect state moves from i to a neighboring tetrahedron, say m' , when the proton in the hydrogen-bond $l'm'$ tunnels to an interstitial position between the tetrahedra i and l' as shown by the arrow.

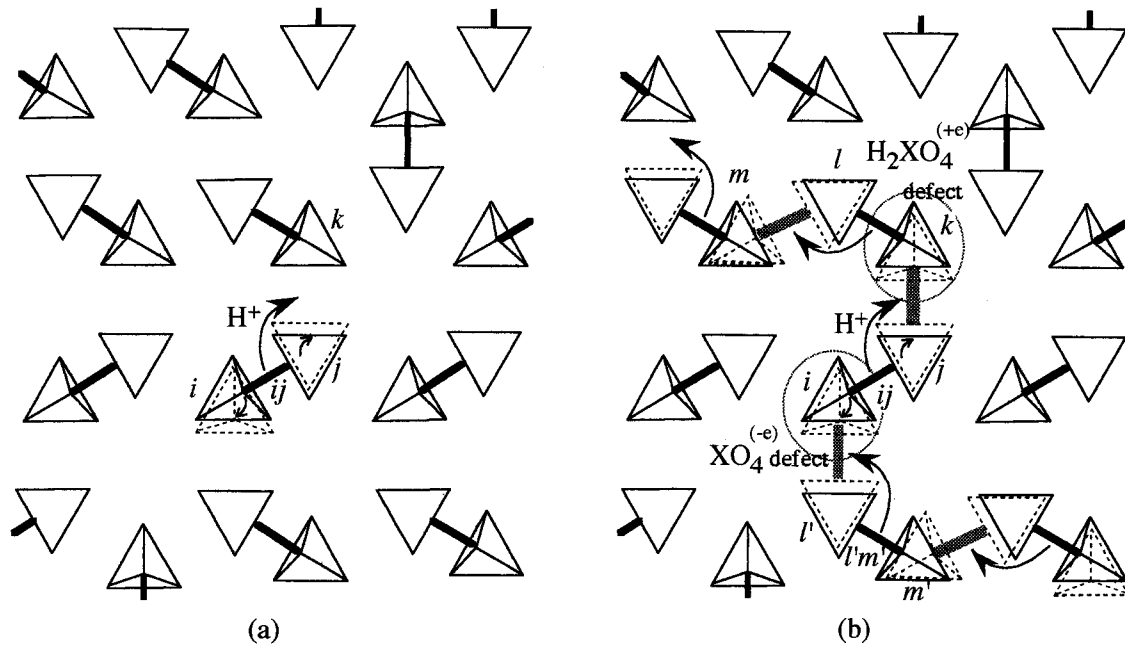


Fig. 2. (a) Schematic view for the breaking of a hydrogen-bond by the rotational displacement of two tetrahedra. (b) Schematic view for the formation of two kinds of defect states, $H_2XO_4^{(+e)}$ and $XO_4^{(-e)}$, and the coherent motion of these defect states due to successive proton tunneling.

In this way, the successive breaking and formation of hydrogen-bonds at different positions appear, and the coherent protonic transport phenomenon takes place.

In closing this section we summarize what we have explained above. First, two kinds of defect states, $H_2XO_4^{(+e)}$ and $XO_4^{(-e)}$, are formed thermally by breaking a hydrogen-bond. Then the $H_2XO_4^{(+e)}$ defect state and the $XO_4^{(-e)}$ defect state move coherently from an XO_4 position to a distant XO_4 position by successive proton tunneling through available sites for protons in hydrogen-bonds like a *chain reaction*. An important feature of this mechanism is that the electrical conduction is not caused by a simple diffusion of protons in ordinary ionic conductors but by the coherent motions of two kinds of defect states.

§3. Theoretical Model

In this section we construct a theoretical model for expressing the coherent motions of two kinds of defect states described in a previous section. In this model the collisions between defect states are neglected. Then we can treat each defect states independently. Let us first pay attention to the motion of a single $H_2XO_4^{(+e)}$ defect state, as shown in Fig. 3(a), where the XO_4 tetrahedra in the paraelastic phase are placed at the equivalent positions, and these positions for a tetrahedron are denoted by i, j , etc. In the present model the sites of protons are taken at the mid-points of hydrogen-bonds for simplicity, because we are investigating a problem of the inter-bond proton hopping, but not the intra-bond motion between double-minima within a hydrogen-bond. Such sites are indicated by circles in this figure, and the notation such as ik is used to show an available site for a proton in the bond between i and k . In this figure the vacant sites and occupied sites of protons are shown by the open and

solid circles, respectively.

Defect states are characterized by their positions and their orientations in a crystal. In Fig. 3(a) those are denoted by α, β , etc. When either of the two protons (the solid circles) in the $H_2XO_4^{(+e)}$ defect state at i -position is transferred to an adjacent site as shown by the solid arrows in Fig. 3(a), the $H_2XO_4^{(+e)}$ defect state moves from i -position to one of the four next-neighboring XO_4 l -, p -, q -, and r -positions, and the state α changes to β, γ, δ , or ν . But the transfer of protons at ik - or ij -site to im -site is excluded, because the state of two defects is energetically unfavorable. As a result the motion of a defect state occurs by the proton tunneling, and the defect state moves resonantly to one of the next-neighboring XO_4 positions one after another, changing the state, say from α to β , and then to γ . Consequently a band-like state is formed. Similarly a band-like state is also formed for the motion of an $XO_4^{(-e)}$ defect state, as shown in Fig. 3(b). In this case the $XO_4^{(-e)}$ defect state can move to one of the three next-neighboring XO_4 positions. Since we can treat the two kinds of defect states in a similar way, here we consider only the motion of the $H_2XO_4^{(+e)}$ defect state in detail, and for the $XO_4^{(-e)}$ defect state only the calculated results are presented.

Choosing the site energy of the defect states as the origin of energy, the model Hamiltonian to describe the coherent motion of the $H_2XO_4^{(+e)}$ defect state is expressed by

$$H = \sum_l \sum_k \sum_i \Gamma a_{kl}^\dagger a_{ik} \left(\sum_j a_{ij}^\dagger a_{ij} - 1 \right), \quad (3.1)$$

where Γ represents the resonant integral of a defect state, in other words, the transfer interaction of a proton be-

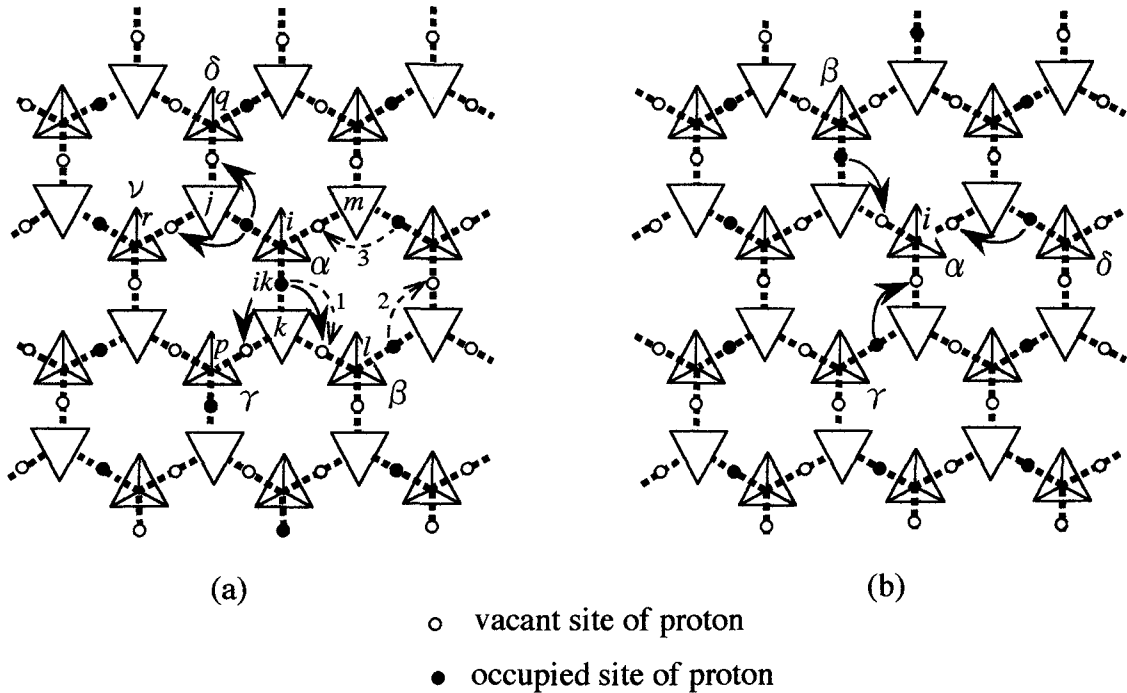


Fig. 3. (a) $\text{H}_2\text{XO}_4^{(+e)}$ defect state is situated at i -position. The possible paths for the transfer motion of the defect state is represented by the solid arrows. (b) $\text{XO}_4^{(-e)}$ state is situated at the i -position.

tween adjacent available sites. The symbols a_{ij}^\dagger and a_{ij} are the creation and annihilation operators of a proton in the site ij , respectively. The factor $(\sum_j a_{ij}^\dagger a_{ij} - 1)$ is 1 when the $\text{H}_2\text{XO}_4^{(+e)}$ defect state lies at the i -position while otherwise zero. As for the $\text{XO}_4^{(-e)}$ state, we can construct the model Hamiltonian in a similar form. Based on this model we will calculate the density of states for the two kinds of defect states and the mobility for the coherent motions of these defect states.

§4. Formulae for the Density of States and the Mobility of the Defect States

In this section we present the formulae to calculate the density of states and the mobility, based on the model Hamiltonian (3.1). Using a basis set for the defect states $|\alpha\rangle$, $|\beta\rangle$, etc., the Green's functions are defined by

$$G_{\beta\alpha}^{(+)}(E) = \left\langle \beta \left| \frac{1}{E + i\epsilon - H} \right| \alpha \right\rangle, \quad (4.1)$$

$$G_{\beta\alpha}(E) = -\frac{1}{\pi} \text{Im} G_{\beta\alpha}^{(+)}(E), \quad (4.2)$$

where E is the energy of a system, and ϵ a positive infinitesimal. As is well-known, the density of states $\rho(E)$ is obtained from the diagonal element of eq. (4.2).

Then we calculate the mobility. For this purpose we introduce the current operator defined by

$$\mathbf{J} = \left(\frac{iq}{\hbar} \right) \sum_{i,j} \Gamma \mathbf{R}_{ji} a_{ji}^\dagger a_{ij} \left(\sum_l a_{il}^\dagger a_{il} - 1 \right), \quad (4.3)$$

where $\mathbf{R}_{ji} = \mathbf{R}_j - \mathbf{R}_i$ with \mathbf{R}_i being the position vector of i -position, and q is the effective charge of a defect. Then the mobility is calculated from the Kubo formula.¹⁹⁾ Calculating the correlation function of current-current oper-

ators and assuming that the system is isotropic within a layer, the mobility μ is expressed in terms of the Green's function as follows:^{20, 21)}

$$\mu = \left(\frac{\pi \hbar}{2qkT} \right) \int e^{-E/kT} \Xi(E) dE \Big/ \int e^{-E/kT} \rho(E) dE, \quad (4.4)$$

where

$$\Xi(E) = -\frac{1}{N} \sum_{\alpha} \sum_{\beta} \sum_{\gamma} \sum_{\delta} G_{\alpha\delta}(E) H_{\delta\gamma} \mathbf{R}_{\delta\gamma} \times G_{\gamma\beta}(E) H_{\beta\alpha} \mathbf{R}_{\beta\alpha}. \quad (4.5)$$

Here k is the Boltzmann constant, T the absolute temperature, N the total number of the defect states, and $\mathbf{R}_{\beta\alpha}$ represents the displacement vector of a defect associated with the change of a state from α to β , which is equal to \mathbf{R}_{li} in Fig. 3(a).

As seen above, the calculations of $\rho(E)$ and μ are ascribed to calculating the Green's function (4.1). We expand it in a power series of H/z . The result is

$$z G_{\beta\alpha}^{(+)}(E) = \delta_{\beta\alpha} + \frac{1}{z} H_{\beta\alpha} + \sum_{\nu=1}^{\infty} \frac{1}{z^{\nu+1}} \sum_{\gamma_1} \sum_{\gamma_2} \cdots \sum_{\gamma_\nu} H_{\beta\gamma_\nu} \cdots H_{\gamma_2\gamma_1} H_{\gamma_1\alpha}, \quad (4.6)$$

where $z = E + i\epsilon$. Let us consider the diagonal element of the Green's function, $G_{\alpha\alpha}^{(+)}$. As shown in eq. (4.6), $(z G_{\alpha\alpha}^{(+)} - 1)$ is equal to the sum of all closed paths which start from a state α and end at the starting state α via intermediate states γ_1 , γ_2 , etc., since only the matrix elements of H between nearest neighbor states are not zero. Thus, we have to find closed paths. This is called

an interaction map.

§5. Interaction Map

When we construct the interaction map from all the closed paths, careful attention should be paid to finding the looping-back-paths which correspond to those returned to the initial state by taking the intermediate states on a loop. It is not hard to find such looping-back-paths in the case of the $H_2XO_4^{(+e)}$ defect state. For example, we can see in Fig. 3(a) that, when a proton moves with three steps around the tetrahedron k clockwise, the defect state at the i -position changes first from the α to β , then to γ , and finally returns to the initial state α . This is called a triangular looping-back-path. It should be noted that there exist no other looping-back-paths except for such triangular paths. Here we should note a case in which, even when a defect state returns to an initial tetrahedron position, the initial state is not necessarily restored. For example, if protons move as indicated by the dotted arrows 1, 2, and 3 in Fig. 3(a), the defect state begins to move from the i -position and returns to the same position i . In this case the initial defect state is not restored, because the configuration of all the protons in the whole crystal is not identical. Thus this is not a looping-back-path.

In this way we can obtain the interaction map for the $H_2XO_4^{(+e)}$ defect state as shown in Fig. 4(a), where the defect states are denoted by vertices. The remarkable characteristic of the interaction map is that the interaction map basically belongs to a category of the Bethe lattice (Cayley tree), though it contains triangular loops. Investigating the $XO_4^{(-e)}$ defect state in a similar way as shown in Fig. 3(b), the interaction map can be obtained as shown in Fig. 4(b). It is clearly seen from this figure that the interaction map for this case is just the Bethe lattice. Here, based on the obtained interaction map for the $H_2XO_4^{(+e)}$ defect state, we can construct the diagrams for $zG_{\alpha\alpha}^{(+)}$. The result is schematically illustrated in Fig. 5, where each defect state and each hopping step are denoted by a vertex with value 1 and a line with Γ/z , respectively.

As a method of summing up the closed paths described in Fig. 5, we employ Haydock's recursion method.^{22, 23)} Here, we give a brief summary of this method. In that method the diagonal element of the Green's function is expressed in a form of a continued fraction. In doing so, a Hamiltonian matrix is transformed to a tridiagonal form by a new basis set $|0\rangle, |1\rangle, |2\rangle, \dots, |n\rangle, \dots$, etc. This new basis set $| \rangle$ is obtained from the original basis set $|0\rangle, |1\rangle, |2\rangle, \dots, |n\rangle, \dots$, etc., which corresponds to the orthonormalized set of the defect states α, β , etc., in the present case, by the following recurrence relation;

$$\begin{aligned} |0\rangle &= |0\rangle \\ b_1|1\rangle &= H|0\rangle - a_0|0\rangle \\ &\vdots \\ b_{n+1}|n+1\rangle &= H|n\rangle - a_n|n\rangle - b_n|n-1\rangle, \quad n \geq 1, \end{aligned} \quad (5.1)$$

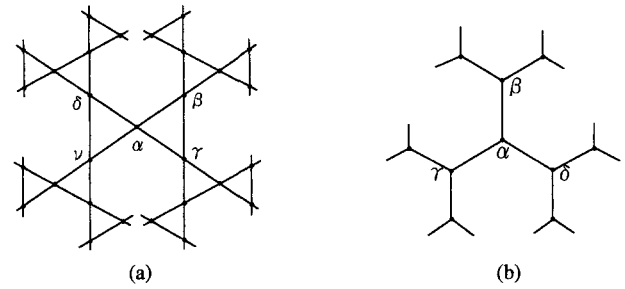


Fig. 4. (a) Interaction map for the $H_2XO_4^{(+e)}$ defect state. (b) Interaction map for the $XO_4^{(-e)}$ defect state.

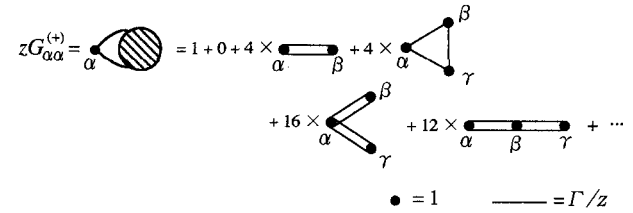


Fig. 5. Diagrams of $zG_{\alpha\alpha}^{(+)}$ for the $H_2XO_4^{(+e)}$ state. Symbol α denotes the starting and terminating vertex, and symbol β and γ denote variable intermediate vertices. The numerical factors before diagrams represent the number of diagrams of respective type.

where a new starting state $|0\rangle$ is chosen as $|0\rangle$. When one obtains $|n+1\rangle$, coefficients a_n and b_n are determined so as for $H|n\rangle$ to orthogonalize to the preceding states $|n\rangle$ and $|n-1\rangle$, and the coefficient b_{n+1} is determined to normalize $|n+1\rangle$ to unity. In the new basis set $|n\rangle$, the Hamiltonian matrix is expressed in the tridiagonal form;

$$\begin{aligned} \langle n|H|n\rangle &= a_n \\ \langle n-1|H|n\rangle &= \langle n|H|n-1\rangle = b_n \\ \langle n|H|m\rangle &= 0 \quad \text{otherwise.} \end{aligned} \quad (5.2)$$

As a result, $\langle 0|(z-H)^{-1}|0\rangle$ can be easily evaluated, and thus one can obtain $G_{00}^{(+)}$ in the following form of the continued fractional representation

$$\begin{aligned} G_{00}^{(+)}(z) &= \langle 0|(z-H)^{-1}|0\rangle \\ &= \frac{1}{z - a_0 - \frac{b_1^2}{z - a_1 - \frac{b_2^2}{\ddots \frac{b_n^2}{z - a_n - b_\infty^2 t(z)}}}}, \end{aligned} \quad (5.3)$$

with

$$t(z) = \frac{1}{z - a_\infty - b_\infty^2 t(z)}. \quad (5.4)$$

In an ordinary case, the a_n and b_n approach quickly to constant values a_∞ and b_∞ when a step n in eq. (5.1) exceeds a certain value n_0 . Thus one can terminate the continued fraction by putting $a_{n_0} = a_\infty$ and $b_{n_0} = b_\infty$. Then the remainder of the continued fraction $t(z)$ can be written as

$$t(z) = \frac{(z - a_\infty) \pm \sqrt{(z - a_\infty)^2 - 4b_\infty^2}}{2b_\infty^2}. \quad (5.5)$$

The (+) sign in eq. (5.5) is rejected, because $t(E + i\epsilon)$ must vanish as $E \rightarrow \infty$ in order that the $G_{00}^{(+)}(z)$ in the form of eq. (5.3) preserve its analytic character of the form E^{-1} at $E \rightarrow \infty$. Thus only the (-) sign in eq. (5.5) is chosen.

§6. Calculated Results

6.1 Density of states

Based on the obtained interaction map and Hamiltonian (3.1), the density of states for the $\text{H}_2\text{XO}_4^{(+e)}$ defect state is calculated by means of the recursion method. When the coefficients a_n and b_n are calculated by the ordinary procedure, the values of a_n and b_n after the second iteration are found not to change. Then we obtain $G_{\alpha\alpha}^{(+)}$ in the following analytic form;

$$G_{\alpha\alpha}^{(+)}(E) = \frac{1}{4\Gamma^2} \frac{1}{z - \frac{\Gamma}{z - \Gamma - 2\Gamma^2 t(z)}}, \quad (6.1)$$

with

$$t(z) = \frac{z - \Gamma - \sqrt{(z - \Gamma)^2 - 8\Gamma^2}}{4\Gamma^2}. \quad (6.2)$$

For the $\text{H}_2\text{XO}_4^{(+e)}$ defect state at certain position, say i , as shown in Fig. 3(a), three configurations are possible with regard to the association of two protons, because the two protons in the defect state can be accommodated in the three available sites around i -position. Since eq. (6.1) has been obtained for a special configuration of protons among the three configurations given in Fig. 3(a), we have to multiply eq. (6.1) by 3 to obtain the density of states. Further, it must be divided by 2 in order to avoid the double counting of paths. As a result, the density of states, $\rho_1(E)$, is obtained as

$$\rho_1(E) = \frac{3}{2} G_{\alpha\alpha}(E). \quad (6.3)$$

The calculated result of $\rho_1(E)$ is plotted as a function of energy E in Fig. 6(a), where the unit of energy is taken as Γ . Here $\rho_1(E)$ satisfies the normalization condition; $\int \rho_1(E) dE = 1$. The calculated width of the density of states is $4\sqrt{2}|\Gamma|$, which is narrower than that of an ordinary square lattice with the same four nearest neighbor sites, since the bandwidth for the ordinary square lattice is $8|\Gamma|$. This means that, since the interaction map belongs basically to a Bethe lattice, the motion of the $\text{H}_2\text{XO}_4^{(+e)}$ defect state has a one-dimensional character. Indeed, two maxima of the density of states near the band edges resemble the shape of the van Hove singularity (two infinities) at the band edges of the one-dimensional band. The shape of $\rho_1(E)$ is asymmetric with respect to $E=0$. This is due to the existence of the closed paths with odd steps, i.e., the triangular looping-back-paths seen in Fig. 4(a). The density of states for the $\text{XO}_4^{(-e)}$ state, $\rho_2(E)$, can be obtained in a similar way. The result is shown in Fig. 6(b). In this case, since there is no closed path with odd steps in the interaction map,

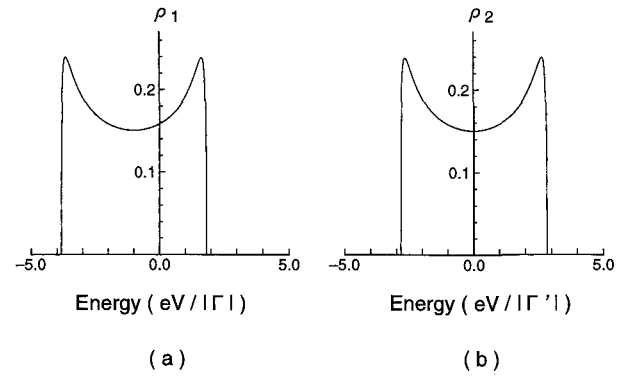


Fig. 6. (a) Density of states for the $\text{H}_2\text{XO}_4^{(+e)}$ defect state where the unit of energy is $|\Gamma|$. (b) Density of states for the $\text{XO}_4^{(-e)}$ defect state where the unit of energy is $|\Gamma'|$.

the shape of $\rho_2(E)$ is symmetric with respect to $E=0$. The width of the density of states is $4\sqrt{2}|\Gamma'|$, where Γ' is the resonant integral of the defect states, $\text{XO}_4^{(-e)}$.

6.2 Mobility

To calculate the mobility of the $\text{H}_2\text{XO}_4^{(+e)}$ defect state, we have first to calculate the off-diagonal element of the Green's function, $G_{\beta\alpha}^{(+)}$ by eq. (4.6). In doing so we sum up all the paths which start from a state α and end at a state β via intermediate states. For convenience, we call the paths which have no any common intermediate states on the route, "irreducible routes". Suppose the length of the shortest path between α and β is m steps. Then $G_{\beta\alpha}^{(+)}$ may be denoted by $G_m^{(+)}$ due to the topological equivalence of vertices in the interaction map. If we consider the case, for example, where m is two as shown in Fig. 7(a), we see that four irreducible routes indicated by line graph exist in Fig. 7(b), where each state and each step on the irreducible routes are denoted by a vertex with value 1 and a line with Γ/z , respectively. We denote the difference between the steps in each irreducible route and those in the shortest route by ℓ . Thus each irreducible route may be characterized by ℓ .

Now it is convenient to introduce the following three quantities defined by ξ , ξ' , and ξ'' : The quantity ξ corresponds to $zG_{\alpha\alpha}^{(+)}$, which has been already obtained in order to calculate the density of states; ξ' and ξ'' correspond to the sums of the closed paths which start from and end at, say γ_2 as shown in Fig. 7(a), but ξ' does not contain a state adjacent to γ_2 , say α , while ξ'' does not contain two states adjacent to γ_2 , say α and γ_1 , on the way. Under these restrictions, ξ' and ξ'' can be calculated by means of the recursion method like the case of ξ . Thus, putting ξ , ξ' , and ξ'' on the irreducible routes so as to avoid double counting of paths as shown in Fig. 7(c), one can express $zG_{m=2}^{(+)}$ as the sum of the four diagrams. We note here that the diagrams with the same ℓ lead to the same expression and that the number of such diagrams with ℓ is ${}_2C_\ell$. Thus, we obtain the following result for $m=2$

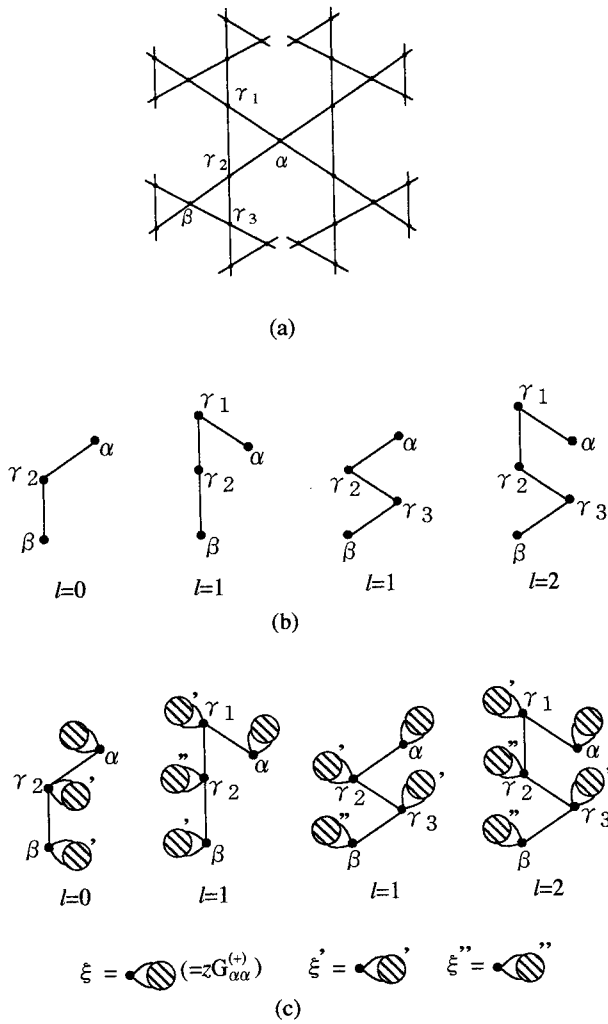


Fig. 7. (a) Interaction map for the $H_2XO_4^{(+e)}$ defect state involving in the calculation of $zG_{\beta\alpha}^{(+)}$. (b) Four irreducible routes for $zG_{\beta\alpha}^{(+)}$ in the case where the length between α and β , m , is two steps. Here ℓ represents the difference between the steps of each irreducible route and that of the shortest one ($\ell=0$). (c) Diagrams of $zG_{\beta\alpha}^{(+)}$ in the present case.

$$zG_{\beta\alpha(m=2)}^{(+)}(E) = {}_2C_0\xi\left(\frac{\Gamma}{z}\right)^2\xi'^2 + {}_2C_1\xi\left(\frac{\Gamma}{z}\right)^{2+1}\xi'^2\xi'' + {}_2C_2\xi\left(\frac{\Gamma}{z}\right)^{2+2}\xi'^2\xi''^2. \quad (6.4)$$

In this way, $zG_{\beta\alpha}^{(+)}$ for a combination of arbitrary α and β is expressed as

$$zG_{\beta\alpha}^{(+)}(E) = zG_m^{(+)} = \sum_{\ell=0}^m {}_mC_{\ell} \xi \left(\frac{\Gamma}{z}\right)^{m+\ell} \xi'^m \xi''^{\ell}. \quad (6.5)$$

Finally we consider the closed paths $\alpha \rightarrow \beta \rightarrow \gamma \rightarrow \delta \rightarrow \alpha$ for the terms in eq. (4.5), $\Xi(E)$. As seen in this equation, a pair α and β and a pair γ and δ are adjacent. Then we can classify the present problem into the following two cases: (I) α, β, γ , and δ are all on a triangular route and (II) otherwise.

In the case (I), four cases further arise. In every case two states among the four states, $\alpha \sim \delta$, are identical

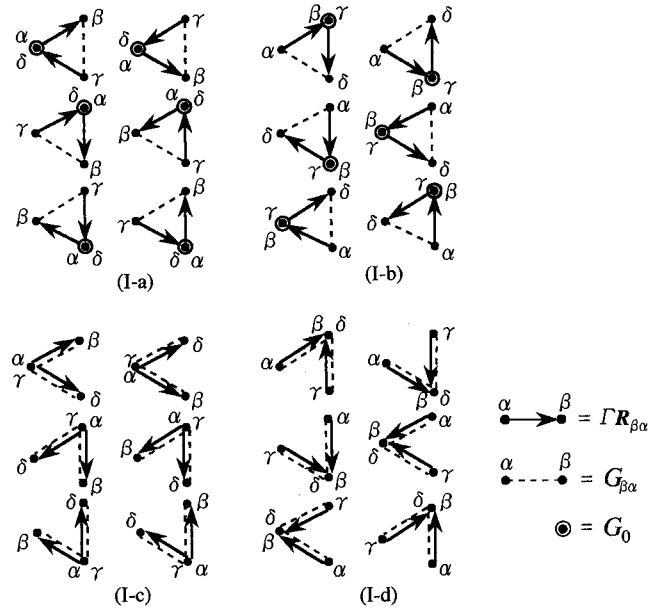


Fig. 8. Diagrams in $N\Xi$ in the case (I).

on a triangular route, i.e., $\alpha=\delta, \beta=\gamma, \alpha=\gamma$, and $\beta=\delta$. Then, 2×3 diagrams for $N\Xi$ on a triangular route are constructed for each of the four cases as shown in Figs. 8(I-a)–8(I-d). Here the factor 3 means the number of ways to choose the starting state α from among the three vertices on the route, and the factor 2 represents the number of ways to choose β as a successive step. The diagrams in the cases (I-a) and (I-b) of Fig. 8 yield the same expression. The same scenario holds for the cases (I-c) and (I-d). Thus the group of (I-a) and (I-b) and that of (I-c) and (I-d) lead to, respectively, the following expressions;

$$2 \times 2 \times 3 \times G_0 G_1 \Gamma^2 \mathbf{R}_{\delta\gamma} \cdot \mathbf{R}_{\beta\alpha}, \quad (6.6)$$

and

$$2 \times 2 \times 3 \times G_1^2 \Gamma^2 \mathbf{R}_{\delta\gamma} \cdot \mathbf{R}_{\beta\alpha}. \quad (6.7)$$

The inner-products appearing in eqs. (6.6) and (6.7) give $R^2 \cos(2\pi/3)$ and $R^2 \cos(\pi/3)$, respectively, where R is $|\mathbf{R}|$. As a result, the terms in $N\Xi$ in eq. (4.5) for the case (I) are calculated as

$$6(G_1^2 - G_0 G_1) \Gamma^2 R^2. \quad (6.8)$$

For the case (II), it is convenient to divide it further into two cases. The first case (II-1) is that no loop appears in the shortest path among the closed paths $\alpha \rightarrow \beta \rightarrow \gamma \rightarrow \delta \rightarrow \alpha$. The second case (II-2) is that loops appear in the shortest path. In the first case, the shortest path $\alpha \rightarrow \beta \rightarrow \gamma \rightarrow \delta \rightarrow \alpha$ lies on a linear route. Let us take the length from one end to another end of a linear route as $m+1$ steps. Then the diagrams for $N\Xi$ are constructed along a linear route with $m+1$ steps as shown in Figs. 9(II-1-a) and 9(II-1-b). The case (II-1-a) shows that the length between β and γ is equal to that between δ and α on the linear route. (Here the case of $m = 0$ is treated later as an exceptional case). These lengths are both m steps. The case (II-1-b) shows that the length between β and γ is different from that

between δ and α on the linear route. One of these is $(m - 1)$ steps, and the other is $(m + 1)$ steps. Thus, the diagrams for the cases (II-1-a) and (II-1-b) are expressed as

$$4 \times G_m^2 \Gamma^2 R_{\delta\gamma} \cdot R_{\beta\alpha}, \quad (6.9)$$

and

$$4 \times G_{m-1} G_{m+1} \Gamma^2 R_{\delta\gamma} \cdot R_{\beta\alpha}, \quad (6.10)$$

respectively. As seen in Figs. 9(II-1-a) and 9(II-1-b), the values of the inner-products appearing in eqs. (6.9) and (6.10) are the same magnitude but with opposite sign to each other, respectively. Hence, the term in $N\Xi$ for the case (II-1) is expressed as

$$4(G_{m-1} G_{m+1} - G_m^2) \Gamma^2 R_{\delta\gamma} \cdot R_{\beta\alpha}. \quad (6.11)$$

As for the exceptional case of $m = 0$, in which α, β, γ , and δ are on a linear route of one step, we can write four diagrams as shown in Fig. 9(II-1-c). Thus $N\Xi$ is expressed as

$$2(G_1^2 - G_0^2) \Gamma^2 R^2. \quad (6.12)$$

In the case (II-2), only one or two loops can be formed in the shortest path among the closed paths $\alpha \rightarrow \beta \rightarrow \gamma \rightarrow \delta \rightarrow \alpha$. For each case, we show examples of diagrams for $N\Xi$ in Figs. 10(II-2-a) and 10(II-2-b). Though eight diagrams can be constructed for each case, we choose here two diagrams for these cases. When we obtain equations corresponding to these diagrams, we find that because the two quantities in each case are the same magnitude but with opposite sign, these cancel each other. The same is true for the remaining diagrams. Thus the case (II-2) has no contribution to $N\Xi$.

Combining eqs. (6.8), (6.11), and (6.12), $\Xi(E)$ is expressed as follows;

$$\begin{aligned} \Xi(E) &= -\frac{3}{2} \times \frac{1}{N} \sum_{(loop)} 6(G_1^2 - G_0 G_1) \Gamma^2 R^2 \\ &\quad - \frac{3}{2} \times \frac{1}{N} \sum_{m=1}^{\infty} \sum_{(m)} 4(G_{m-1} G_{m+1} - G_m^2) \Gamma^2 R_{\delta\gamma} \cdot R_{\beta\alpha} \\ &\quad - \frac{3}{2} \times \frac{1}{N} \sum_{(0)} 2(G_1^2 - G_0^2) \Gamma^2 R^2, \end{aligned} \quad (6.13)$$

where a reason for the appearance of the factor $3/2$ is the same as the reason that the factor $3/2$ has appeared in the expression for the density of states, $\rho_1(E)$. The symbol $\sum_{(m)}$ represents the summation taken over the linear routes of $(m+1)$ steps under the restriction mentioned above, $\sum_{(0)}$ the summation taken over the linear routes of 1 step, and $\sum_{(loop)}$ the summation taken over the triangular routes. These can be written as

$$\sum_{(m)} = N \times 4 \times 2 \times 2 \times \cdots \times \frac{1}{2} = 2^{m+1} N, \quad (6.14)$$

$$\sum_{(0)} = N \times 4 \times \frac{1}{2} = 2N, \quad (6.15)$$

$$\sum_{(loop)} = 2N \times \frac{1}{3} = \frac{2}{3} N, \quad (6.16)$$

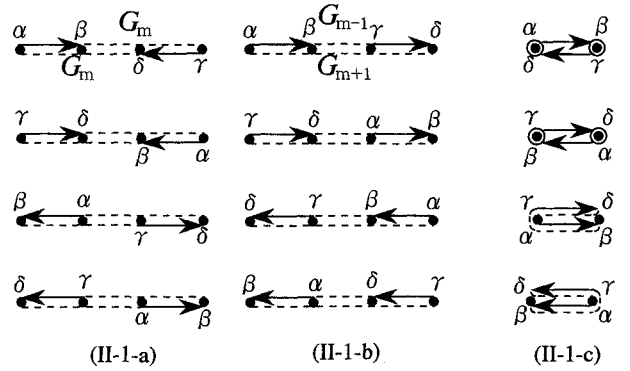


Fig. 9. (II-1-a) and (II-1-b): Diagrams in $N\Xi$ for a linear route of $(m + 1)$ steps in the case (II-1). (II-1-c): Diagrams in $N\Xi$ for a linear route of 1 step.

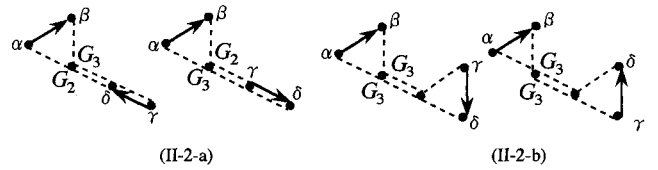


Fig. 10. Examples of diagrams in $N\Xi$ in the case (II-2). In (II-2-a) and (II-2-b) one and two loops are formed in the shortest path among closed paths $\alpha \rightarrow \beta \rightarrow \gamma \rightarrow \delta \rightarrow \alpha$, respectively.

where $1/2$ appearing in eqs. (6.14) and (6.15), and $1/3$ appearing in eq. (6.16) are the factors which are needed for avoiding double counting of paths. The remaining problem is to calculate $R_{\delta\gamma} \cdot R_{\beta\alpha}$ in eq. (6.13) for the case (II-1). The direction for successive transfers of a defect state is random. Therefore, when a defect moves by changing the state from α to β , then from β to β_1, \dots and finally from γ to δ along the linear route of $m+1$ steps without repeating identical states, the ensemble average of the inner-product of the first and the last displacement vectors $R_{\delta\gamma} \cdot R_{\beta\alpha}$ is simply expressed as $R^2(1/3)^m$. This randomness in the direction for transfers of a defect plays an important role in attaining a finite mobility, because no other scattering mechanism is assumed in the present model. Thus, eq. (6.13) is written as

$$\begin{aligned} \Xi(E) &= -\frac{3}{2} \times 4(G_1^2 - G_0 G_1) \Gamma^2 R^2 \\ &\quad - \frac{3}{2} \times \sum_{m=1}^{\infty} \left(\frac{2}{3}\right)^m 8(G_{m-1} G_{m+1} - G_m^2) \Gamma^2 R^2 \\ &\quad - \frac{3}{2} \times 4(G_1^2 - G_0^2) \Gamma^2 R^2. \end{aligned} \quad (6.17)$$

As for the $XO_4^{(-e)}$ defect state, case (I) is not present. Therefore Ξ can be calculated analytically.

Assuming both $|I|$ and $|I'| \ll kT$, the mobility μ for the coherent motion of the $H_2XO_4^{(+e)}$ state is calculated from eqs. (4.4), (6.3), and (6.17), while the mobility μ' for the coherent motion of the $XO_4^{(-e)}$ state is also calculated in a similar way. The obtained results are

$$\left\{ \begin{aligned} \mu &= \frac{q|I|R^2}{\hbar kT} \times 1.070 \\ &\quad \text{for the } H_2XO_4^{(+e)} \text{ defect state,} \\ \mu' &= \frac{|q'|I'|R^2}{\hbar kT} \times 1.066 \\ &\quad \text{for the } XO_4^{(-e)} \text{ defect state,} \end{aligned} \right. \quad (6.18)$$

where q and q' are the effective charges of an $H_2XO_4^{(+e)}$ defect state and an $XO_4^{(-e)}$ defect state, respectively. When we investigate the contribution from each term in Ξ in eq. (6.17) to the mobility in detail, we find that, for the case of the $H_2XO_4^{(+e)}$ defect state, the contribution from the first term in the right hand side of eq. (6.17) is negligible, and that the second and third terms contribute approximately to a half of the total magnitude of mobility. The same is true for the $XO_4^{(-e)}$ defect state, though a term which corresponds to the first term in eq. (6.17) is not present. As seen in eq. (6.18), we notice that the mobility has the form of Einstein relation in its temperature dependence. From this result one can say that the defect state, for example the $H_2XO_4^{(+e)}$ defect state, hops successively with the diffusion constant $D = R^2|\Gamma|/\hbar \times 1.070$. However it should be noted that the motion of the defect state is not simply a classical random hopping but a coherent hopping in the present model. In this sense it is a quantum mechanical phenomenon.

Now, let us calculate the conductivity. In doing so we recall that two kinds of defect states are formed thermally by breaking a hydrogen-bond within a layer. Thus the concentration of defects, n , is expressed in the form of the Boltzmann distribution,

$$n = N e^{-E_a/kT}, \quad (6.19)$$

where E_a is the formation energy for creating simultaneously an $H_2XO_4^{(+e)}$ defect state and an $XO_4^{(-e)}$ defect state thermally by breaking a hydrogen-bond. Thus, from eqs. (6.18) and (6.19) the static conductivity is obtained as follows;

$$\begin{aligned} \sigma &= qn(\mu + \mu') \\ &= \frac{q^2 R^2 N (1.070|\Gamma| + 1.066|\Gamma'|)}{\hbar kT} e^{-E_a/kT}. \end{aligned} \quad (6.20)$$

The obtained conductivity obeys the Arrhenius' equation, which is consistent with experimental results.

We estimate the magnitude of σ for the case of $Rb_3H(SeO_4)_2$. From experimental results¹¹⁾ we obtain $E_a = 0.26$ eV, $R = 5.8 \times 10^{-8}$ cm, and $T_c = 450$ K. Then assuming that $q=q'=e$, $n_0=10^{22}$ cm⁻³, and $|\Gamma|=|\Gamma'|=10^{-5}$ eV, we estimate the mobility as 2.6×10^{-4} cm²/Vsec. Thus the conductivity has the order of a magnitude of 10^{-3} Ω^{-1} cm⁻¹.

§7. Summary and Concluding Remarks

In this paper, a new mechanism of ionic conductivity in the high temperature paraelastic phase of the $M_3H(XO_4)_2$ [$M=Rb, Cs, X=S, Se$] has been proposed. The key features of the mechanism are the following two: (1) Two kinds of defect states, $H_2XO_4^{(+e)}$ and $XO_4^{(-e)}$, are formed thermally by breaking a hydrogen-bond. This thermal activation process is the origin for the observed Arrhenius' equation in the temperature dependence of conductivity; (2) the $H_2XO_4^{(+e)}$ defect state and the $XO_4^{(-e)}$ defect state move coherently from an XO_4 position to a distant XO_4 position as the result of the successive proton tunneling among hydrogen-bonds. In this sense the proton conduction has a quantum mechanical

nature. In fact, in obtaining the Green's function for the present model, the characteristic paths, called interaction map, have appeared. We have showed that the interaction maps are essentially a Bethe lattice. Based on the present model, the density of states and the mobility have been calculated both for the coherent motions of the $H_2XO_4^{(+e)}$ defect state and the $XO_4^{(-e)}$ defect state. The density of states shows the characteristic feature of a one-dimensional band, reflecting the feature of the Bethe lattice. We have further showed that, even though the hopping motion of the defect states is coherent, the mobility has the form of Einstein relation, i.e., its temperature dependence is of $1/T$ form.

Finally a remark is made on the mechanism of phonon-assisted tunneling proposed by Yamada and Ikeda for explaining dynamical properties of protons in KH_2PO_4 . Although we have assumed that the energies before and after the tunneling of a proton is equal, in reality the XO_4 tetrahedra vibrate and rotate around sites i, j, k , etc., so that the energies before and after the tunneling might not be equal. In that case the phonon-assisted tunneling plays an important role for the $M_3H(XO_4)_2$ like KH_2PO_4 . We hope that the neutron incoherent scattering experiments will elucidate a mechanism of proton tunneling in $M_3H(XO_4)_2$ in the near future.

Acknowledgments

We would like to thank Dr. M. Komukae, Miss J. Hatori, and Prof. T. Osaka for many valuable discussions.

- 1) R. Blinc: J. Phys. Chem. Solids **13** (1960) 204.
- 2) M. Tokunaga and T. Matsubara: Prog. Theor. Phys. **35** (1966) 581.
- 3) E. Matsushita: J. Phys. Soc. Jpn. **62** (1993) 2074; *ibid.* **62** (1993) 2079.
- 4) Y. Yamada and S. Ikeda: J. Phys. Soc. Jpn. **63** (1994) 3691.
- 5) Y. Yamada: J. Phys. Soc. Jpn. **63** (1994) 3756.
- 6) M. Ichikawa and K. Motida: Phys. Rev. B **36** (1987) 874.
- 7) Y. Noda *et al.*: J. Phys. Soc. Jpn. **61** (1992) 905.
- 8) A. I. Baranov, L. A. Shuvalov and N. M. Shchagina: JETP Lett. **36** (1982) 459.
- 9) A. I. Baranov *et al.*: Sov. Phys. Crystallogr. **32** (1987) 400.
- 10) A. I. Baranov *et al.*: Sov. Phys. Solid State **29** (1987) 1448.
- 11) A. I. Baranov *et al.*: Solid State Ionics **36** (1989) 279.
- 12) M. Komukae *et al.*: J. Phys. Soc. Jpn. **59** (1990) 197.
- 13) R. Mizeris *et al.*: Sov. Phys. Crystallogr. **36** (1991) 385.
- 14) R. Blinc *et al.*: Phys. Status Solidi B **123** (1984) K83.
- 15) Yu. N. Moskvich, A. M. Polyakov and A. A. Sukhovskij: Sov. Fiz. Tverd. Tela **30** (1988) 45.
- 16) Yu. N. Moskvich, A. M. Polyakov and A. A. Sukhovskij: Ferroelectrics **81** (1989) 197.
- 17) N. M. Plakida and W. Salejda: Phys. Status Solidi B **148** (1988) 473.
- 18) A. Pawlowski and Cz. Pawlaczyk: Ferroelectrics **81** (1988) 201.
- 19) R. Kubo: J. Phys. Soc. Jpn. **12** (1957) 570.
- 20) T. Matsubara and Y. Toyozawa: Prog. Theor. Phys. **26** (1961) 739.
- 21) I. Minagawa: J. Phys. Soc. Jpn. **35** (1973) 357.
- 22) R. Haydock, V. Heine and M. J. Kelly: J. Phys. C **5** (1972) 2845.
- 23) R. Haydock, V. Heine and M. J. Kelly: J. Phys. C **8** (1975) 2591.